Journal of Electrical and Electronic Engineering
2022; 10(3): 71-79
http://www.sciencepublishinggroup.com/j/jeee
doi: 10.11648/j.jeee.20221003.11
ISSN: 2329-1613 (Print); ISSN: 2329-1605 (Online)

Fiber Fuse Simulation in Hollow-Core Photonic Crystal Fibers

Yoshito Shuto

Ofra Project, Iruma City, Japan

Email address:
ofra@tuba.ocn.ne.jp

To cite this article:
Yoshito Shuto. Fiber Fuse Simulation in Hollow-Core Photonic Crystal Fibers. *Journal of Electrical and Electronic Engineering*. Vol. 10, No. 3, 2022, pp. 71-79. doi: 10.11648/j.jeee.20221003.11

Received: May 2, 2022; **Accepted**: May 17, 2022; **Published**: May 26, 2022

Abstract: Recently great interest has been aroused by the development of photonic crystal fibers (PCFs). Hollow-core photonic crystal fibers (HC-PCFs) can guide light inside the hollow core by photonic bandgap or inhibited-coupling mechanisms. HC-PCFs exhibit low propagation losses at 1.064 μm and the 1.51-1.60 μm range. The HC-PCFs are now implemented as an important tool of laser beam delivery in place of traditional single mode optical fibers. One of the problems arising from high-power injection in the optical fiber is the probability of triggering the fiber fuse effect. This effect is related to a heat conduction process in optical fibers. The unsteady-state thermal conduction process in several HC-PCFs (revolver fibers) for high-power transmission was studied theoretically by the explicit finite-difference method using the thermochemical SiO_x production model. For heat conduction analysis, the complicated inner structure of revolver fiber was simplified using the model composed of silica-ring and air-hole layers. The calculated velocities of fiber fuse propagation in two types of polymer-coated revolver fibers were in fair agreement with the experimental values. If the polymer coating of the revolver fiber is removed, the Fresnel reflection at the outer surface of the support tube occurs and the back-reflected light wave is incident upon the silica capillaries and the hollow core. To clarify the in-phase condition, we estimated phase changes of optical routes in the uncoated revolver fiber. It was found that the reflected waves from the outer surfaces of the silica capillary and support tube are in phase at the core-capillary boundary, and they are mutually enhanced as a consequence of the constructive interference. As a result, the power in the hollow core and the silica capillary was improved for the uncoated revolver fiber compared with the polymer-coated one. The calculated velocity of fiber fuse propagation in the uncoated revolver fiber was in fair agreement with the experimental value.

Keywords: Fiber Fuse Phenomenon, Hollow-Core Photonic Crystal Fiber, Finite-Difference Technique

1. Introduction

Recently great interest has been aroused by the development of photonic crystal fibers (PCFs) [1-16]. In PCFs, a microstructured or photonic crystal material forms the fiber cladding. The core in which the light propagates is formed by omitting one or more periods of the photonic crystal (leaving an air core) or by filling in one or more air holes (forming a solid core). The former is called a hollow-core PCF (HC-PCF) and the latter is called a holey fiber (HF) or a microstructured optical fiber (MOF).

Hollow-core photonic crystal fibers (HC-PCFs) can guide light inside the hollow core by photonic bandgap (PBG) [8] or inhibited-coupling (IC) mechanisms [15]. Furthermore, the relationship between the negative curvature and the confinement loss in the HC-PCF family has been experimentally and theoretically investigated by several research institutes [17-29]. Pryamikov *et al*. fabricated a novel hollow-core PCF with a negative curvature of the core boundary and a cladding consisting of one row of capillaries [17]. This fiber is often called a negative curvature fiber [18-23], an antiresonant fiber [24-27], or a revolver fiber [28, 29].

Recently, Sakr *et al.* reported the fabrication of the nested antiresonant nodeless hollow-core fiber (NANF) with a record low loss of 0.51 dB/km at 1.064 μm [30] and Jasion *et al*. reported the minimum loss of 0.28 dB/km between 1.51 and 1.60 μm in the NANF [31].

The HC-PCFs can provide a large light-gas interaction overlap inside hollow-core [5, 11] and wide transmission bands [10], exhibiting the potential for improving gas detection performance

[32] and realizing a high-performance gas fiber laser [33-40].

On the other hand, the use of high-power lasers in the industry has been rapidly advanced by incorporating flexible-fiber-based beam delivery. The laser beams cannot be transported through traditional step-index fibers as their peak intensity lies above the damage threshold of silica and would therefore destroy the fiber itself. The HC-PCFs are now implemented as a tool of laser beam delivery in place of traditional optical fibers [41-47].

One of the problems arising from these high-power levels injected in the optical fiber is the probability of detonating the fiber fuse effect. This phenomenon was discovered by British researchers in 1987-1988 [48, 49] in conventional single-mode optical fibers. The fiber fuse effect in revolver fibers [50, 51] has been reported.

In this paper, we investigated the generation of a fiber fuse and its propagation in revolver fibers by the explicit finite-difference method using the thermochemical SiO_x production model [52].

2. Fiber Fuse Effect in Revolver Fibers

The occurrence of a fiber fuse in a revolver fiber was first reported in 2018 by Kolyadin *et al*. [50].

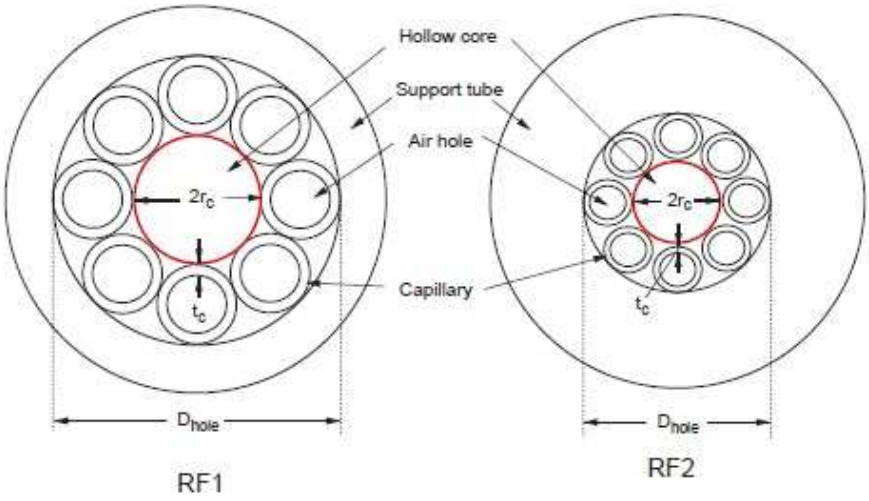

Figure 1. *Two types of revolver fiber.*

They fabricated the two types of revolver fibers (RF1 and RF2) shown in Figure 1. Both fibers have a relatively simple air-silica cladding structure, which consists of one layer of capillaries. In RF1, these capillaries touch each other, whereas they are located at a certain distance in RF2.

In Figure 1, the hollow core radius r_c, the inner diameter of the support tube D_{hole}, and the capillary thickness t_c of RF1/RF2 are 42/20 μm, 93/36 μm, and 3.1/0.8 μm, respectively. The support tube diameter ($2r_f$) of RF1/RF2 is 125/100 μm.

2.1. Laser Source for Fiber Fuse Experiments

The fiber fuse experiments were carried out using a pulse laser operated at a wavelength (λ_0) of 1.064 μm. The laser radiation consisted of nanosecond trains of picosecond pulses (NTPPs) and had the duration of 130 ns.

The fiber fuse initiation was observed in RF1 and RF2 at the average powers of about 4 W (RF1) and about 2 W (RF2), and the fiber fuse propagated at a velocity of about 1 m/s.

The threshold power corresponded to the average intensity of 2.4×10^9 W/cm^2 (RF1) and 5.2×10^9 W/cm^2 (RF2) over the duration of the NTPP.

These values were one order of magnitude smaller than the breakdown threshold intensity I_B (8.2×10^{10} W/cm^2 [53]) for air, which was estimated for the 10 ns pulsed laser operated at $\lambda_0 = 1.064$ μm.

For a revolver fiber, it is known that the extinction ratio of the power in the center of the hollow core to that in the silica capillary is more than 20 dB [25]. This means that the theoretical optical power overlap ratio between the core and the cladding, η, becomes less than 1%.

If η of 0.5% is assumed for the revolver fiber, the intensities I_s near the silica capillaries in RF1 and RF2 can be estimated to be 12 MW/cm^2 (RF1) and 26 MW/cm^2 (RF2) over the duration of the NTPP.

These values are of the same magnitude as the threshold intensity I_{th} (about 1-10 MW/cm^2) observed in the fiber fuse experiments using a CW laser operated at $\lambda_0 = 1.064$ μm [54].

2.2. Fiber Fuse Initiation in Revolver Fiber

In the fiber fuse experiments, a planar absorbing metal (absorbent) surface was brought parallel to the fiber end face [50]. In what follows, we used copper as the absorbing metal. When the laser beam was focused on the absorbent, the temperature of the laser-illuminated spot on the absorbent rose.

The optical absorption coefficient α is related to the extinction coefficient k and λ_0 by [55]

$$\alpha = 4\pi k/\lambda_0 \quad (1)$$

A value of $k = 6.22$ for copper at $\lambda_0 = 0.96$ μm has been reported [56]. Using Eq. (1) and this k value, we estimated

the absorption coefficient of copper to be $\alpha = 7.35 \times 10^7$ m^{-1} at $\lambda_0 = 1.064$ μm. This value is about three orders of magnitude larger than the α values (10^4 m^{-1} order) required for fiber fuse generation.

The part of the silica capillaries in contact with the heated absorbent is also heated by thermal conduction and radiation from the absorbent, as described in [57]. Then, this part starts to absorb the laser beam because of its absorption enhancement due to the temperature rise.

The heated part of the capillaries also heats the surrounding area, which also starts to absorb the laser beam. As this process is repeated, the heated spot will move backward (toward the light source), as observed by Kolyadin *et al*. [50].

In the following section, we describe the unsteady-state thermal conduction process in a revolver fiber theoretically by the explicit finite-difference method on the basis of the thermochemical SiO_x production model [52].

3. Fiber Fuse Calculation in Revolver Fibers

We used the simplified model shown in Figure 2 for heat conduction analysis of the revolver fiber. This model is similar to the multi-layered model proposed by Wang and Ding [23]. However, our model simplified the structure of revolver fiber, compared with their multi-layered model.

The hollow core was assumed to be a cylindrical rod of diameter $2r_c$ and it was surrounded by a suitably designed cladding of high (silica ring) and low (air hole) refractive indices.

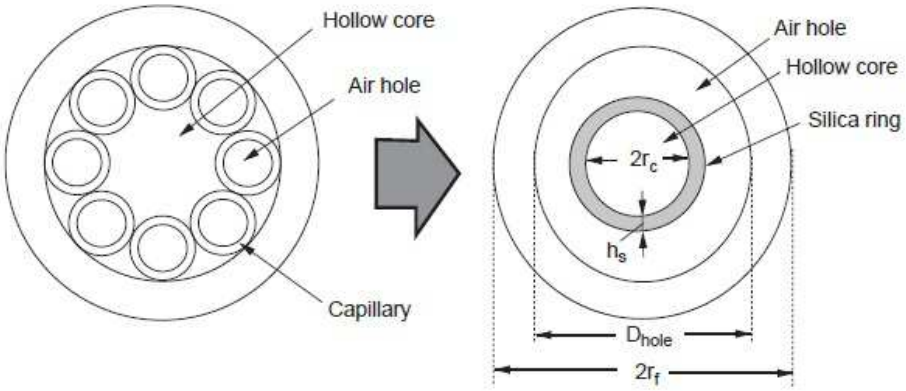

Figure 2. *Heat conduction model for revolver fiber RF1.*

The hollow core and air hole layer were assumed to be filled with air at the same temperature as the surrounding air (T_a). We used the following values of λ (W m^{-1} K^{-1}), ρ (kg m^{-3}), and C_p (J kg^{-1} K^{-1}) of air in the heat conduction calculation [58].

$$\lambda = 0.105$$

$$\rho = 0.183$$

$$C_p = 1{,}306$$

3.1. Fiber Fuse Propagation in RF1

In an actual revolver fiber RF1, eight capillaries of silica glass exist in the air-silica cladding, and the air-filling fraction η_s of the cladding structure is about 68%. If the width h_s of the silica ring is set to 11 μm (~D_{hole}/8), η_s becomes about 66%. This η_s is slightly smaller than that (68%) of an actual RF1.

Using the model described above, we investigated the appearance of the fiber fuse effect in a revolver fiber by the explicit finite-difference method.

We assumed that the revolver fiber is in an atmosphere of temperature $T = T_a$ and part of the silica ring of length ΔL (= 40 μm) is heated to a temperature of T^0_c (> T_a), as shown in Figure 3.

In the calculation, we set the time interval δt to 10 ns, the step size along the r axis δr to r_f/20, and the step size along the z axis δz to 20 μm and assumed that $T^0_c = 3{,}000$ K and $T_a = 298$ K.

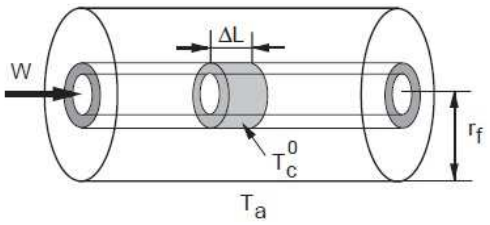

Figure 3. *Hot zone in silica ring of revolver fiber.*

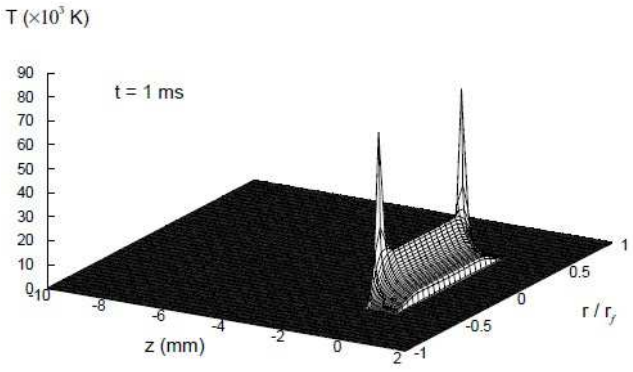

Figure 4. *Temperature field in RF1 after 1 ms when I = 18 MW/cm^2 at λ_0 = 1.064 μm.*

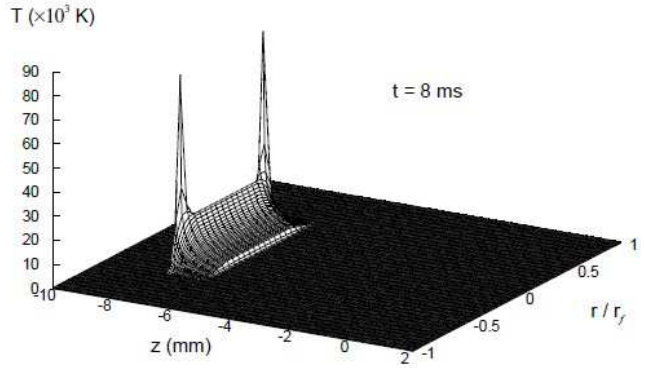

Figure 5. *Temperature field in RF1 after 8 ms when I = 18 MW/cm² at λ_0 = 1.064 μm.*

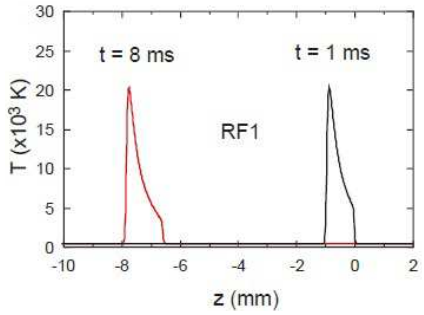

Figure 6. *Temperature fields of core center of RF1 after 1 ms and 8 ms when I = 18 MW/cm² and λ_0 = 1.064 μm.*

We estimated the temperature field T (r, z) of the revolver fiber RF1 at t = 1 ms and 8 ms after the incidence of laser light with I = 18 MW/cm^2 (= 1.5I_s) and λ_0 = 1.064 μm.

The calculated temperature fields are shown in Figures 4 and 5. As shown in Figure 4, the temperature of the silica-ring center near the end of the hot zone (z = -0.96 mm) increases abruptly to about 7.1 × 10^4 K after 1 ms. The heated part of the silica ring heats air molecules in the hollow core, in which the temperature also starts to increase. This rapid rise in the temperature initiates the fiber fuse propagation, as shown in Figure 5. After 8 ms, the high-temperature front in the silica-ring center reaches a z value of -7.84 mm. The average propagation velocity V_f was estimated to be 0.98 m/s using these data. This value is close to the V_f (1.0 m/s) observed by Kolyadin *et al.* [50] and is also the same value as that (~1 m/s) of the SMF28 optical fiber [54].

The temperature fields of the core center along the z direction were calculated at t = 1 ms and 8 ms after the incidence of laser light with I = 18 MW/cm^2 and λ_0 = 1.064 μm. The calculated results are shown in Figure 6. The heat generated in the silica-ring layer is transferred to the neighboring core layers of the RF1. At a time of 1 ms after laser light incidence, a peak temperature (T_p) of 2.0 × 10^4 K or above occurs in the center of the hollow-core layer. The T_p value is maintained after 8 ms, as shown in Figure 6. The propagation velocity of the heated air is the same as that (0.98 m/s) of fiber fuse propagation.

3.2. Fiber Fuse Propagation in Polymer-Coated RF2

Next, we investigated the unsteady-state thermal conduction process in the revolver fiber RF2 theoretically by the explicit finite-difference method. We used the simplified model shown in Figure 2 for heat conduction analysis of the revolver fiber RF2.

In an actual revolver fiber RF2, eight capillaries of silica glass exist in the air-silica cladding, and the air-filling fraction η_s of the cladding structure is about 79%. If the width h_s of the silica ring is set to 5 μm (~D_{hole}/7), η_s becomes about 44%. This η_s is smaller than that (79%) of an actual RF2.

We assumed that the revolver fiber RF2 is in an atmosphere of temperature $T = T_a$, and part of the silica ring of length ΔL (= 40 μm) is heated to a temperature of T^0_c (> T_a), as shown in Figure 3.

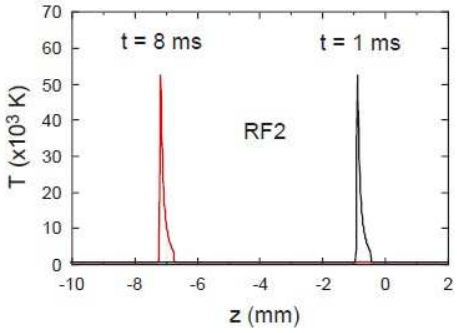

Figure 7. *Temperature fields of core center of RF2 after 1 ms and 8 ms when I = 24 MW/cm² and λ_0 = 1.064 μm.*

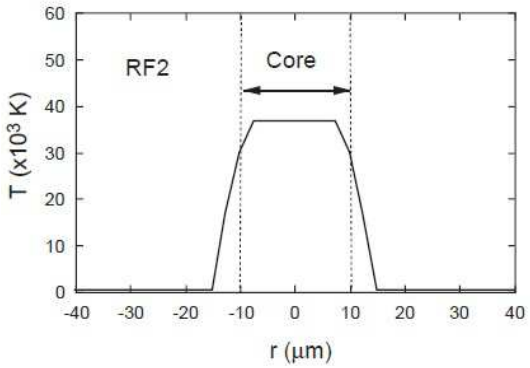

Figure 8. *Temperature field near high-temperature front of RF2 after 1 ms when I = 24 MW/cm² and λ_0 = 1.064 μm.*

In the calculation, we set the time interval δt to 5 ns, the step size along the r axis δr to r_f/20, and the step size along the z axis δz to 20 μm, and assumed that T^0_c = 3,000 K and T_a = 298 K.

We estimated the temperature fields of the core center of the revolver fiber RF2 along the z direction at t = 1 ms and 8 ms after the incidence of laser light with I = 24 MW/cm^2 (= 0.93I_s) and λ_0 = 1.064 μm. The calculated results are shown in Figure 7. As shown in Figure 7, the core center temperature near the end of the hot zone (z = -0.86 mm) increases abruptly to about 5.2 × 10^4 K after 1 ms. This rapid rise in the temperature initiates the fiber fuse propagation. After 8 ms, the high-temperature front in the core center reaches a z value of -7.14 mm. The average propagation

velocity V_f was estimated to be 0.90 m/s using these data. This value is close to the V_f (0.91 m/s) observed by Kolyadin *et al*. [50]. In RF2, the T_p value (5.2×10^4 K) is maintained after 8 ms, as shown in Figure 7.

The temperature field near the high-temperature front after the incidence of laser light with I = 24 MW/cm^2 was calculated along the r direction at t = 1 ms. The calculated result is shown in Figure 8. As shown in the figure, the temperatures in the hollow core are higher than 3×10^4 K, and the temperatures in the silica-ring layer decrease with increasing r and reach ~T_a at the end of the silica-ring layer.

The temperature distribution shown in Figure 8 is similar to the intensity distribution of optical-discharge plasma radiation in RF2 (Figure 5(b) in [50]) observed by Kolyadin *et al*.

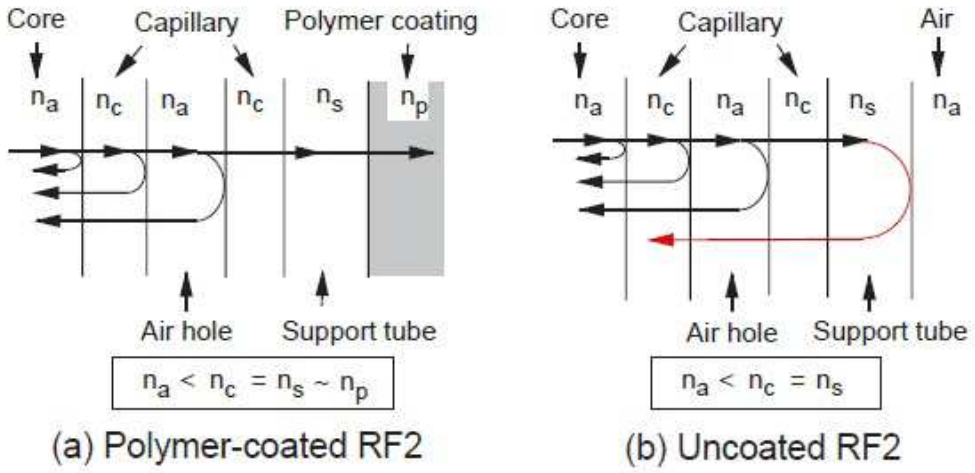

Figure 9. *Schematic of light localization in core of polymer-coated RF2 (a) and uncoated RF2 (b).*

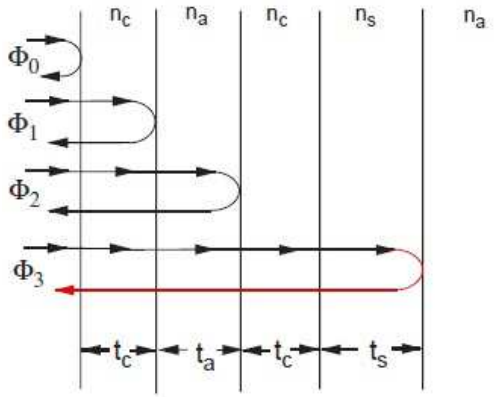

Figure 10. *Optical routes in core of polymer-coated or uncoated RF2.*

3.3. Fiber Fuse Propagation in Uncoated RF2

If RF2 was completely covered with a polymer coating, the measured V_f was 0.91 m/s [50]. However, if the polymer coating was partially removed and the silica support tube directly bordered air, the measured V_f became 2.84 m/s, which was three times larger than that of the polymer-coated RF2 [51].

RF2 consists of a hollow core and an air-silica cladding, which contains one layer of silica capillaries (see Figure 1). In this fiber, the transverse components of a light wave along the radial direction propagate from the core to the silica capillary, and are then sent back to the core after being reflected at the core-capillary boundary and the inner and outer surfaces of the silica capillaries, as shown in Figure 9(a),

If the polymer coating of the RF2 is removed, the Fresnel reflection at the outer surface of the support tube occurs and the back-reflected light wave is incident upon the silica capillaries and the hollow core, as shown in Figure 9(b).

If all or several of the reflected waves stated above are in phase at the core-capillary boundary, then they are mutually enhanced as a consequence of constructive interference. To clarify the in-phase condition, we estimated four phase changes Φ_0-Φ_3 of optical routes shown in Figure 10. Among them, Φ_3 is solely related to the uncoated RF2.

The phase change is accumulated by the radial translation and an additional phase change Φ_R due to the reflection [59].

Φ_R depends on the relative magnitude in the refractive indices of layers situated at both sides of the interface. If a light wave travels from a low-index material to a high-index material, Φ_R becomes 0. Therefore, Φ_0 in Figure 10 leads to 0.

On the contrary, Φ_R becomes π when a light wave travels from a high-index material to a low-index material.

To determine the phase change due to radial translation, we need the lateral propagation constants denoted by

$$k_i = 2\pi\sqrt{n_i^2 - n_{eff}^2} \;/\; \lambda_0 \;\; (i = a,\ c,\ s) \qquad (2)$$

where n_{eff} is the effective index of the least lossy mode of RF2 and λ_0 (= 1.064 μm) is the wavelength of the light wave.

As n_{eff} of the fundamental mode is close to n_a (= 1.0) [60, 61] at λ_0 = 1.064 μm, Eq. (2) becomes

$$k_i \approx 2\pi\sqrt{n_i^2 - 1} \,/\, \lambda_0 \;\; (i = a,\ c,\ s) \qquad (3)$$

The refractive index n of pure silica can be calculated using the Sellmeier equation:

$$n^2 - 1 = \sum_{i=1}^{3} c_i \lambda^2_0 \,/\, (\lambda^2_0 - b_i) \quad (4)$$

where c_i and b_i are the parameters listed in Table 1 [62].

Table 1. *Sellmeier parameters of pure silica [62].*

Parameters	Pure SiO_2
c_1	0.6965325
c_2	0.4083099
c_3	0.8968766
b_1	0.004368309
b_2	0.01394999
b_3	97.93399

The n value of pure silica at λ_0 = 1.064 μm was calculated to be 1.44988 using Eq. (4). Therefore, in the calculation, we used $n_c = n_s = 1.452$ for the silica capillary and silica support tube at λ_0 = 1.064 μm. We also used $n_a = 1.0$, $t_c = 0.8$ μm, t_a = 6.4 μm, and t_s = 32.0 μm.

Let us consider the phase change Φ_1-Φ_3 shown in Figure 10. To satisfy the in-phase condition responsible for Φ_0, waves reflected from the outer and inner surfaces of the silica capillary and the inner surface of the support tube must satisfy the following relations (Bragg conditions):

$$\Phi_1 - \Phi_0 = 2\, k_c\, t_c + \pi = 2\, \pi\, m_1 \quad (5)$$

$$\Phi_2 - \Phi_0 = 2\, (k_c\, t_c + k_a\, t_a) = 2\, \pi\, m_2 \quad (6)$$

$$\Phi_3 - \Phi_0 = 2\, (k_c\, t_c + k_a\, t_a + k_c\, t_c + k_s\, t_s) + \pi = 2\, \pi\, m_3 \quad (7)$$

where m_1, m_2, and m_3 are integers.

By substituting Eq. (3) into Eqs. (5-7), the following equations are derived:

$$nt_1 \equiv 4 \sqrt{n_c^2 - 1}\; t_c = (2\, m_1 - 1)\, \lambda_0 \quad (8)$$

$$nt_2 \equiv 2 \sqrt{n_c^2 - 1}\; t_c = m_2\, \lambda_0 \quad (9)$$

$$nt_3 \equiv 4\, (2 \sqrt{n_c^2 - 1}\; t_c + \sqrt{n_s^2 - 1}\; t_s) = (2\, m_3 - 1)\, \lambda_0 \quad (10)$$

We calculated nt_1-nt_3 and estimated m_1-m_3 using Eqs. (8-10). The calculated results are shown in Table 2.

Table 2. *Calculated parameters of phase conditions.*

Parameter	Unit	Value
nt_1	μm	3.369
nt_2	μm	1.684
nt_3	μm	141.491
m_1	-	2.08
m_2	-	1.58
m_3	-	66.99

As shown in this table, m_2 (= 1.58) is not an integer, but m_1 (= 2.08) and m_3 (= 66.99) can be regarded as the integers 2 and 67.

This means that the reflected waves from the outer surfaces of the silica capillary and support tube are in phase at the core-capillary boundary, and they are mutually enhanced as a consequence of the constructive interference.

As a result, the power in the hollow core and the silica capillary will be improved for the uncoated RF2 compared with the polymer-coated RF2. If the gain in power of 5 dB is assumed for the uncoated RF2, the intensity I_s near the silica capillaries in the uncoated RF2 can be estimated to be 76 MW/cm^2 over the duration of the NTPP.

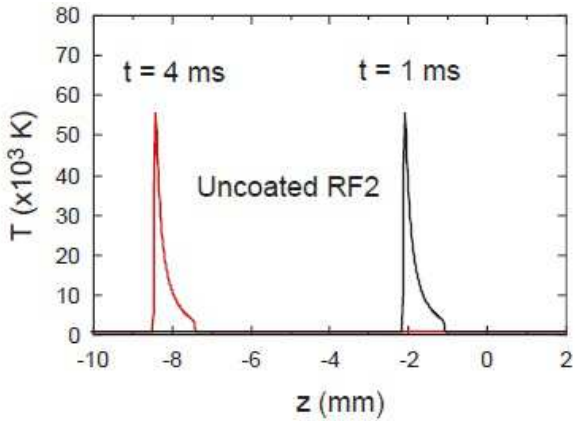

Figure 11. *Temperature fields of core center of uncoated RF2 after 1 ms and 4 ms when I = 76 MW/cm^2 and λ_0 = 1.064 μm.*

We estimated the temperature fields of the core center of the uncoated RF2 along the z direction at t = 1 ms and 4 ms after the incidence of laser light with I = 76 MW/cm^2 and λ_0 = 1.064 μm. The calculated results are shown in Figure 11.

As shown in Figure 11, the core center temperature near the end of the hot zone (z = -2.06 mm) increases abruptly to about 5.5 × 10^4 K after 1 ms. This rapid rise in the temperature initiates the fiber fuse propagation. After 4 ms, the high-temperature front in the core center reaches a z value of -8.38 mm. The average propagation velocity V_f was estimated to be 2.11 m/s using these data. This value is close to the V_f (2.84 m/s) observed by Bufetov *et al.* [51].

In the uncoated RF2, the T_p value (5.5 × 10^4 K) is maintained after 4 ms, as shown in Figure 11.

4. Cavity Formation in Revolver Fiber

When a fiber fuse was generated in RF2, the damage was in the form of periodic (or nonperiodic) cavities remaining in the fiber, and the periodic cavity interval Λ of the damage was about 170 μm [50] or 180 μm [51]. The periodicity of the cavities was sometimes significantly disturbed [51].

This Λ is about one order larger than that (13-22 μm) [63, 64] observed in conventional single-mode optical fibers (SMFs) with a CW laser source.

When CW laser light is incident upon an SMF, heat generated continuously at the hot zone in the core layer owing to light absorption and the temperature of this part rises to 1 × 10^4 K and above. Then the thermal wave increases in size and starts to propagate in the negative z direction toward the light source. In this process, the periodic cavities with (relatively) small Λ values are formed in the SMF.

The relationship between the heat penetration time t_p and temperature penetration thickness δ in a silica glass layer is given by [65].

$$\delta \sim 3.6\sqrt{kt_p} \quad (11)$$

where k is the thermal diffusivity. k values of silica glass at 500 K and 3,000 K are 4.40×10^{-6} m^2/s and 8.32×10^{-8} m^2/s, respectively. The relationship between t_p and δ in a silica glass layer was investigated at 500 K and 3,000 K.

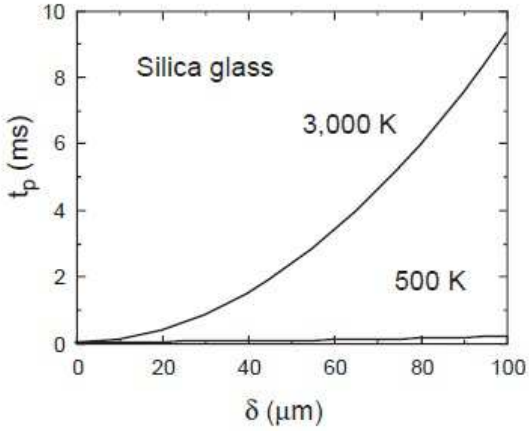

Figure 12. *Relationship between t_p and δ in silica glass layer.*

The calculated results are shown in Figure 12. As shown in this figure, t_p values increase with increasing δ and the t_p values at 3,000 K are larger than those at 500 K. The t_p value at δ = 60 μm is about 3.3 ms at 3,000 K.

In the fiber fuse experiments of the RF2, a Nd:YAG laser with a repetition rate of 1,200 Hz was used as a pulse laser source. This means that the period of the NTPP is about 0.83 ms. This period is shorter than the heat penetration time (3.3 ms) through a 60-μm-thick glass layer.

On the other hand, it is well known that the first cavity length of fiber fuse propagation is a large value of 160-180 μm [64]. The duration of NTPPs is 130 ns [50, 51]. This duration is about one-tenth the time (18-30 μs) [64] for the formation of second (short) cavity from the first long cavity during fiber fuse propagation.

When an NTPP is incident upon the RF2, heat generated at the silica capillary owing to light absorption is transmitted to the adjacent part of the capillary, and the temperature of the part rises to 3,000 K. Then the thermal wave increases in size and starts to propagate in the negative z direction toward the light source. In this way, the first long cavity is formed in the RF2. Then the heat in the capillaries is efficiently transferred in the air of the adjacent core and the long cavity is frozen after a quick shutdown of the laser source until the next NTPP arrives at RF2 after 0.83 ms. In this way, the formation of a long cavity with a large Λ (about 170 μm or 180 μm) is allowed to continue for each incidence of the NTPP upon the RF2.

5. Conclusion

The unsteady-state thermal conduction process in several hollow-core photonic crystal fibers (HC-PCFs) was studied theoretically by the explicit finite-difference method using the thermochemical SiO_x production model. For heat conduction analysis, the complicated inner structure of HC-PCFs was simplified using the model composed of silica-ring and air-hole layers. The calculated velocities of fiber fuse propagation in several revolver fibers were in fair agreement with the experimental values.

References

[1] Birks T. A., Roberts P. J., Russell P. St. J., Atkin D. M., and Shepherd T. J. (1995). Full 2-D photonic bandgaps in silica/air structures. Electron. Lett., 31 (22), 1941-1943.

[2] Knight J. C., Birks T. A., Russell P. St. J., and Atkin D. M. (1996). All-silica single-mode optical fiber with photonic crystal cladding. Opt. Lett., 21 (19), 1547-1549.

[3] Birks T. A., Knight J. C., and Russell P. St. J. (1997). Endlessly single-mode photonic crystal fiber. Opt. Lett., 22 (13), 961-963.

[4] Knight J. C., Birks T. A., Russell P. St. J., and de Sandro J. P. (1998). Properties of photonic crystal fiber and the effective index model. J. Opt. Soc. Am. A, 15 (3), 748-752.

[5] Knight J. C., Broeng J., Birks T. A., and Russell P. St. J. (1998). Photonic band gap guidance in optical fibers. Science, 282, 1476-1478.

[6] Cregan R. F., Mangan B. J., Knight J. C., Birks T. A., Russell P. St. J., Roberts P. J., and Allan D. C. (1999). Single-mode photonic band gap guidance of light in air. Science, 285, 1537-1539.

[7] Broeng J., Mogilevstev D., Barkou S. E., and Bjarklev A. (1999). Photonic crystal fibers: a new class of optical waveguides. Opt. Fiber Technol., 5, 305-330.

[8] Russell P. St. J. (2003). Photonic crystal fibers. Science, 299, 358-362.

[9] Knight J. C. (2003). Photonic crystal fibres. Nature, 424, 847-851.

[10] Vienne G., Xu Y., Jackobsen C., Deyerl H., Jensen J. B., Sorensen T., Hansen T. P., Huang Y., Terrel M., Lee R. K., Mortensen N. A., Broeng J., Simonsen H., Bjarkey A., and Yariv A. (2004). Ultra-large bandwidth hollow-core guiding in all-silica Bragg fibers with nano-supports. Opt. Express, 12 (15), 3500-3508.

[11] Roberts P. J., Couny F., Sabert H., Mangan B. J., Williams D. P., Farr L., Mason M. W., Tomlinson A., Birks T. A., Knight J. C., and Russell P. St. J. (2005). Ultimate low loss of hollow-core photonic crystal fibers. Opt. Express, 13 (1), 236-244.

[12] Russell P. St. J. (2006). Photonic-crystal fibers. IEEE J. Lightwave Technol., 24 (12), 4729-4749.

[13] Benabid F. (2006). Hollow-core photonic bandgap fibre: new light guidance for new science and technology. Philos. Trans. R. Soc. A, 364, 3439-3462.

[14] Knight J. C. (2007). Photonic crystal fiber and fiber lasers. J. Opt. Soc. Am. B, 24 (8), 1661-1668.

[15] Couny F., Benabid F., Roberts P. J., Light P. S., and Raymer M. G. (2007). Generation and photonic guidance of multi-octave optical-frequency combs. Science, 318, 1118-1121.

[16] Debord B., Amrani F., Vincetti L., Gérôme F., and Benabid F. (2019). Hollow-core fiber technology: the rising of 'gas photonics'. Fibers, 7, 16-1-16-58.

[17] Pryamikov A. D., Biriukov A. S., Kosolapov A. F., Plotnichenko V. G., Semjonov S. L., and Dianov E. M. (2011). Demonstration of a waveguide regime for a silica hollow-core microstructured optical fiber with a negative curvature of the core boundary in the spectral region > 3.5 μm. Opt. Express, 19 (2), 1441-1448.

[18] Kosolapov A. F., Pryamikov A. D., Biriukov A. S., Shiryaev V. S., Astapovich M. S., Snopatin G. E., Plotnichenko V. G., Churbanov M. F., and Dianov E. M. (2011). Demonstration of CO_2-laser power delivery through chalcogenide-glass fiber with negative-curvature hollow core. Opt. Express, 19 (25), 25723-25728.

[19] Kolyadin A. N., Kosolapov A. F., Prymikov A. D., Biriukov A. S., Plotnichenko V. G., and Dianov E. M. (2013). Light transmission in negative curvature hollow core fiber in extremely high material loss region. Opt. Express, 21 (8), 9514-9519.

[20] Yu F. and Knight J. C. (2013). Spectral attenuation limits of silica hollow core negative curvature fiber. Opt. Express, 21 (18), 21466-21471.

[21] Yu F. and Knight J. C. (2016). Negative curvature hollow-core optical fiber. IEEE J. Selected Top. Quantum Electron., 22 (2), 4400610.

[22] Wei C., Weiblen R. J., Menyuk C. R., and Hu J. (2017). Negative curvature fibers. Ad. Opt. Photon., 9 (3), 504-561.

[23] Wang Y. and Ding W. (2017). Confinement loss in hollow-core negative curvature fiber: A multi-layered model. Opt. Express, 25 (26), 33122-33133.

[24] Belardi W. and Knight J. C. (2014). Hollow antiresonant fibers with reduced attenuation. Opt. Lett., 30 (7), 1853-1856.

[25] Poletti F. (2014). Nested antiresonant nodeless hollow core fiber. Opt. Express, 22 (20), 23807-23828.

[26] Belardi W. (2015). Design and properties of hollow antiresonant fibers for the visible and near infrared spectral range. IEEE J. Lightwave Technol., 33 (21), 4497-4503.

[27] Yu F., Xu M., and Knight J. C. (2016). Experimental study of low-loss single-mode performance in anti-resonant hollow-core fibers. Opt. Express, 24 (12), 12969-12975.

[28] Kosolapov A. F., Alagashev G. K., Kolyadin A. N., Pryamikov A. D., Biryukov A. S., Bufetov I. A., and Dianov E. M. (2016). Hollow-core revolver fibre with a double-capillary reflective cladding. Quantum Electron., 46 (3), 267-270.

[29] Bufetov I. A., Kosolapov A. F., Pryamikov A. D., Gladyshev A. V., Kolyadin A. N., Krylov A. A., Yatsenko Y. P., and Biriukov A. S. (2018). Revolver hollow core optical fibers. Fibers, 6, 39-1-39-26.

[30] Sakr H., Chen Y., Jasion G. T., Bradley T. D., Hayes J. R., Mulvad H. C. H., Davidson I. A., Fokoua E. N., and Poletti F. (2020). Hollow core optical fibres with comparable attenuation to silica fibres between 600 and 1100 nm. Nat. Commun., 11, 6030.

[31] Jasion G. T., Bradley T. D., Harrington K., Sakr H., Chen Y., Fokoua E. N., Davidson I. A., Taranta A., Hayes J. R., Richardson D. J., and Poletti F. (2020). Hollow core NANF with 0.28 dB/km attenuation in the C and L bands. Proc. Opt. Fiber Conf. (OFC 2020), Th4B.4.

[32] Yu R., Chen Y., Shui L., and Xiao L. (2020). Hollow-core photonic crystal fibers gas sensing. Sensors, 20, 2996.

[33] Nampoothiri A. V. V., Jones A. M., Fourcade-Dutin C., Mao C., Dadashzadeh N., Baumgart B., Wang Y. Y., Alharbi M., Bradley T., Campbell N., Benabid F., Washburn B. R., Corwin K. L., and Rudolph W. (2012). Hollow-core optical fiber gas lasers (HOFGLAS): a review. Opt. Mat. Express, 2 (7), 948-961.

[34] Benoit A., Ilinova E., Beaudou B., Debord B., Gerôme F., and Benabid F. (2017). Spectral-temporal dynamics of high power Raman picosecond pulse using H_2-filled kagome HC-PCF. Opt. Lett., 42 (19), 3896-3899.

[35] Cao L., Gao S., Peng Z., Wang X., Wang Y., and Wang P. (2018). High peak power 2.8 μm Raman laser in a methane-filled negative-curvature fiber. Opt. Express, 26 (5), 5609-5615.

[36] Li Z., Huang W., Cui Y., and Wang Z. (2018). Efficient mid-infrared cascade Raman source in methane-filled hollow-core fibers operating at 2.8 μm. Opt. Lett., 43 (19), 4671-4674.

[37] Gladyshev A. V., Kosolapov A. F., Khudyakov M. M., Yatsenko Y. P., Kolyadin A. N., Krylov A. A., Pryamikov A. D., Biriukov A. S., Likhachev M. E., Bufetov I. A., and Dianov E. M. (2018). 2.9, 3.3, and 3.5 μm Raman lasers based on revolver hollow-core silica fiber filled by $^1H_2/D_2$ gas mixture. IEEE J. Selected Topics Quantum Electron., 24 (3), 0903008.

[38] Astapovich M. S., Gladyshev A. V., Khudyakov M. M., Kosolapov A. F., Likhachev M. E., and Bufetov I. A. (2019). Watt-level nanosecond 4.42-μm Raman laser based on silica fiber. IEEE Photon. Technol. Lett., 31 (1), 78-81.

[39] Wang Y., Dasa M. K., Adamu A. I., Antonio-Lopez J. E., Habib M. S., Amezcua-Correa R., Bang O., and Markos C. (2020). High pulse energy and quantum efficiency mid-infrared gas Raman fiber laser targeting CO_2 absorption at 4.2 μm. Opt. Lett., 45 (7), 1938-1941.

[40] Gladyshev A., Yatsenko Y., Kolyadin A., Kompanets V., and Bufetov I. (2020). Mid-infrared 10-μJ-level sub-picosecond pulse generation via stimulated Raman scattering in a gas-filled revolver fiber. Opt. Mat. Express, 10 (12), 3081-3089.

[41] Beaudou B., Gerôme F., Wang Y. Y., Alharbi M., Bradley T. D., Humbert G., Auguste J.-L., Blondy J.-M., and Benabid F. (2012). Millijoule laser pulse delivery for spark ignition through kagome hollow-core fiber. Opt. Lett., 37 (9), 1430-1432.

[42] Jaworski P., Yu F., Maier R. R. J., Wadsworth W. J., Knight J. C., Shephard J. D., and Hand D. P. J. (2013). Picosecond and nanosecond pulse delivery through a hollow-core negative curvature fiber for micro-machining applications. Opt. Express, 21 (19), 22742-22753.

[43] Ulrich A., Maier R. R. J., Yu F., Knight J. C., Hand D. P. J., and Shephard J. D. (2013). Flexible delivery of Er:YAG radiation at 2.94 μm with negative curvature silica glass fibers: a new solution for minimally invasive surgical procedures. Biomedical Opt. Express, 4 (2), 193-205.

[44] Dumitrache C., Rath J., and Yalin A. P. (2014). High power spark delivery system using hollow core kagome lattice fibers. Materials, 7, 5700-5710.

[45] Michieletto M., Lyngso J. K., Jakobsen C., Laegsgaard J., Bang O., and Alkeskjold T. T. (2016). Hollow-core fibers for high power pulse delivery. Opt. Express, 24 (7), 7103-7119.

[46] Elizer S. and Wedel B. (2018). Hollow core optical fibers for industrial ultra short pulse laser beam delivery applications. Fibers, 6, 80-1-80-11.

[47] Zhu X., Wu D., Wang Y., Yu F., Li Q., Qi Y., Knight J., Chen S., and Hu L. (2021). Delivery of CW laser power up to 300 Watts at 1080 nm by an uncooled low-loss ant-resonant hollow-core fiber. Opt. Express, 29 (2), 1492-1501.

[48] Kashyap R. and Blow K. J. (1988). Observation of catastrophic self-propelled self-focusing in optical fibres. Electron. Lett., 24 (1), 47-49.

[49] Hand D. P. and Russell P. St. J. (1988). Solitary thermal shock waves and optical damage in optical fibers: the fiber fuse. Opt. Lett., 13 (9), 767-769.

[50] Kolyadin A. N., Kosolapov A. F., and Bufetov I. A. (2018). Optical discharge propagation along hollow-core optical fibres. Quantum Electron., 48 (12), 1138-1142.

[51] Bufetov I. A., Kolyadin A. N., Kosolapov A. F., Efremov V. P., and Fortov V. E. (2019). Catastrophic damage in hollow core optical fibers under high power laser radiation. Opt. Express, 27 (13), 18296-18311.

[52] Shuto Y. (2015). Simulation of fiber fuse phenomenon in single-mode optical fibers. In Advances in Optical Fiber Technology, Eds. Yasin M., Arof H., and Harun S. W. Chap. 5, InTech, Rijeka.

[53] Sticker J. and Parker J. G. (1982). Experimental investigation of electrical breakdown in nitrogen and oxygen induced by focused laser radiation at 1.064 μ. J. Appl. Phys., 53 (2), 851-855.

[54] Davis D. D., Mettler S. C., and DiGiovani D. J. (1996). A comparative evaluation of fiber fuse models. Proc. Soc. Photo-Opt. Instrum. Eng., 2966, 592-606.

[55] Jensen B. (1985). The quantum extension of the Drude-Zener theory in polar semiconductors. In Handbook of Optical Constants of Solids, Ed. Palik E. D., Chap. 9. Academic Press Inc., New York.

[56] Ordal M. A., Long L. L., Bell R. J., Bell S. E., Bell R. R., Alexander, Jr. R. W., and Ward C. A. (1983). Optical properties of metals Al, Co, Cu, Au, Fe, Pb, Ni, Pd, Pt, Ag, Ti, and W in the infrared and far infrared. Appl. Opt., 22 (7), 1099-1119.

[57] Shuto Y. (2016). End face damage and fiber fuse phenomena in single-mode fiber-optic connectors. J. Photonics, 2016, 2781392.

[58] Shoji M. (1995). Heat Transfer Textbook, Appendix F, University of Tokyo Press, Tokyo.

[59] Sakai J. and Suzuki Y. (2011). Equivalence between in-phase and antiresonant reflection conditions in Bragg fiber and its application to antiresonant reflecting optical waveguide-type fibers. J. Opt. Soc. Am. B, 28 (1), 183-192.

[60] Argyros A. (2002). Guided modes and loss in Bragg fibres. Opt. Express, 10 (24), 1411-1417.

[61] Deng A., Hasan M. I., Wang Y., and Chang W. (2020). Analyzing mode index mismatch and field overlap for light guidance in negative-curvature fibres. Opt. Express, 28 (19), 27974-27988.

[62] Shibata N. and Edahiro T. (1982). Refractive-index dispersion for GeO_2-, P_2O_5- and B_2O_3-doped silica glasses in optical fibers. Trans. IECE Jpn., E65 (3), 166-172.

[63] Atkins R. M., Simpkins P. G., and Yabon A. D. (2003). Track of a fiber fuse: a Rayleigh instability in optical waveguides. Opt. Lett., 28 (12), 974-976.

[64] Todoroki S. (2014). Fiber Fuse: Light-Induced Continuous Breakdown of Silica Glass Optical Fiber, Chap. 3, NIMS Monographs, Springer, Tokyo.

[65] Shoji M. (1995). Heat Transfer Textbook, Chap. 4, University of Tokyo Press, Tokyo.